

Molecular reorientation in hydrogen-bonding liquids: through algebraic $\sim t^{-3/2}$ relaxation toward exponential decay

M. F. Gelin and D. S. Kosov

*Department of Chemistry and Biochemistry,
University of Maryland, College Park, 20742, USA*

Abstract

We present a model for the description of orientational relaxation in hydrogen-bonding liquids. The model contains two relaxation parameters which regulate the intensity and efficiency of dissipation, as well as the memory function which is responsible for the short-time relaxation effects. It is shown that the librational portion of the orientational relaxation is described by an algebraic $\sim t^{-3/2}$ contribution, on top of which more rapid and non-monotonous decays caused by the memory effects are superimposed. The long-time behavior of the orientational relaxation is exponential, although non-diffusional. It is governed by the rotational energy relaxation. We apply the model to interpret recent molecular dynamic simulations and polarization pump-probe experiments on *HOD* in liquid D_2O [C. J. Fecko et al, *J. Chem. Phys.* 122, 054506 (2005)].

I. INTRODUCTION

The recent advances in nonlinear ultrafast polarization-sensitive spectroscopy¹ make it possible to monitor molecular rotation in hydrogen-bonding liquids in real time^{2,3,4,5,6,7,8,9,10,11}. Due to the enormous complexity of the problem, which is exacerbated by many-body effects and multitudes of the time scales involved, experimental data alone are insufficient for understanding the underlying dynamics. Nowadays, molecular dynamic has become a standard tool for studying molecular reorientation in liquids¹². Furthermore, one can even use *ab initio* molecular dynamics (in which the density functional theory is invoked to describe molecular electronic structure and inter- and intramolecular forces are calculated on-the-fly)^{13,14} or centroid molecular dynamics (which accounts for quantum effects/corrections)¹⁵. On the other hand, there exists a plenty of "old" phenomenological models of molecular reorientation in gases and liquids. We mention the small-angle rotational diffusion model^{16,17,18}, the jump diffusion model^{19,20,21,22}, the friction model^{23,24,25}, the Gaussian cage model^{26,27}, the itinerant oscillator model²⁸, along with the more sophisticated memory function approach (^{28,29,30,31,32,33} and references therein), the extended diffusion models^{34,35,36,37,38,39,40,41,42}, the rotational Fokker-Planck equation^{24,35,36,43,44,45,46}, the confined rotator model⁴⁷, the Steele model⁴⁸, the Keilson-Storer model (KSM)^{33,35,49,50,51,52,53}, the fluctuating/stochastic cage model^{33,54,55,56,57}, and the generalized Langevin equations/normal mode approach^{28,29,33,58}. Furthermore, the model has been elaborated¹¹, which accounts for the effects of rotation-vibration coupling in ensembles of hydrogen-bonding molecules on the time-resolved pump-probe signals. Very recently, the generalized jump model of water reorientation has been suggested⁵⁹. The models, of course, rely upon a simplified picture of molecular rotation. However, in contrast with molecular dynamics simulations, they get a deep insight into physics of molecular reorientation, give a clear perception of rotational relaxation and provide us with explicit formulas for the pertinent correlation functions (CFs).

The aim of the present paper is to develop a simple and physically sound model of molecular reorientation in hydrogen-bonding liquids. The model is intended to supply experimentalists with a simple theory to interpret and to fit their data and to clarify the interconnection of orientational relaxation and hydrogen bond making/breaking processes. In hydrogen-bonding liquids, the angular momentum CFs exhibit pronounced oscillations and

orientational CFs (OCFs) display a rapid short-time decay followed by a slower (sometimes oscillatory) pattern which transforms gradually into a monotonous exponential relaxation. By incorporating the proper description of the memory effects into the KSM framework, we developed a non-Markovian generalization of thereof, NKSM. Within the NKSM, we derived analytical expressions for the angular momentum and energy CFs, as well as simple recursive expressions for OCFs.

The paper is structured as follows. The NKSM is formulated in Sec.II. The explicit expressions for the angular momentum CF, rotational energy CF and OCFs are presented and discussed in Sec.III. Sec.IV contains illustrative calculations of various NKSM CFs and comparisons with the results of molecular dynamic simulations and polarization pump-probe experiments on *HOD* in D_2O at a room temperature⁵. A brief summary of the main findings can be found in Sec. V. Appendix A contains the explicit formulas for the calculation of spherical and linear rotor OCFs within the NKSM. Analytical expressions for OCFs in a particular case of “perfect” librations are obtained and discussed in Appendix B.

A few words about the notation and conventions. (i) The reduced variables are used throughout the article: time, angular momentum and energy are measured in units of $\sqrt{I/(k_B T)}$, $\sqrt{I k_B T}$ and $k_B T$, respectively. Here k_B is the Boltzmann constant, T is the temperature, and I is a characteristic moment of inertia of the molecule so that $\tau_r = \sqrt{I/(k_B T)}$ is the averaged period of free rotation. (ii) All Laplace-transformed operators are denoted by tilde, viz. $\tilde{f}(s) = \int_0^\infty dt \exp\{-st\}f(t)$ for $\forall f(t)$. (iii) Repeated dummy Greek indexes imply summation over x , y and z .

II. THE MODEL

We start with a formally exact Zwanzig-type master equation, which can be derived from the general N -particle rotation-translational Liouville equation by applying the projection operator technique^{22,60,61}

$$\partial_t \rho(\mathbf{J}, \boldsymbol{\Omega}, t) = -i\hat{\Lambda}(\mathbf{J}, \boldsymbol{\Omega})\rho(\mathbf{J}, \boldsymbol{\Omega}, t) - \int_0^t dt' \hat{C}(\mathbf{J}, \boldsymbol{\Omega}, t-t')\rho(\mathbf{J}, \boldsymbol{\Omega}, t'). \quad (1)$$

Here $\rho(\mathbf{J}, \boldsymbol{\Omega}, t)$ is the single particle probability density function, \mathbf{J} is the angular momentum in the molecular frame, $\boldsymbol{\Omega}$ are the Euler angles which specify orientation of the molecular frame with respect to the laboratory one. The free-rotor Liouville operator consists of the

two contributions,

$$\hat{\Lambda}(\mathbf{J}, \boldsymbol{\Omega}) = \hat{\Lambda}_{\boldsymbol{\Omega}} + \hat{\Lambda}_{\mathbf{J}}, \quad (2)$$

which describe, respectively, the angular momentum driven reorientation and the angular momentum change during free rotation:

$$\hat{\Lambda}_{\boldsymbol{\Omega}} = I_{\alpha}^{-1} J_{\alpha} \hat{L}_{\alpha}, \quad \hat{\Lambda}_{\mathbf{J}} = -i \varepsilon_{\alpha\beta\gamma} I_{\beta}^{-1} J_{\alpha} J_{\beta} \partial_{J_{\gamma}}. \quad (3)$$

I_{α} are the main moments of inertia, \hat{L}_{α} are the angular momentum operators in the molecular frame. For linear and spherical rotors, $\hat{\Lambda}_{\mathbf{J}} \equiv 0$.

The relaxation operator \hat{C} assumes the form

$$\hat{C}(\mathbf{J}, \boldsymbol{\Omega}, t) = \hat{C}(\mathbf{J}) g(t), \quad (4)$$

$g(t)$ being the memory function which is normalized to unity, $\int_0^{\infty} dt g(t) = \tilde{g}(0) = 1$. All the formulas derived in the present paper are valid for any functional form of $g(t)$. Since a simple exponential memory function is known to exaggerate oscillatory effects in the angular momentum CF and OCFs (see, e.g.,^{25,29,32,50}), the two-exponential memory function will be adopted for making all specific calculations, viz.,

$$g(t) = \sigma \lambda_1 \exp\{-\lambda_1 t\} + (1 - \sigma) \lambda_2 \exp\{-\lambda_2 t\}, \quad (5)$$

$$\tilde{g}(s) = \frac{\sigma \lambda_1}{s + \lambda_1} + \frac{(1 - \sigma) \lambda_2}{s + \lambda_2}. \quad (6)$$

The parameters λ_i regulate the memory effects of the two contributions, and σ controls their relative significance. If we let both λ_1 and λ_2 tend to infinity, then $g(t) \rightarrow \delta(t)$ and the Markovian limit is recovered.

Since molecules are massive inertial particles, the relaxation operator $\hat{C}(\mathbf{J})$ is assumed to be $\boldsymbol{\Omega}$ -independent⁶². This is tantamount to the statement that molecular reorientation is driven by the (time-dependent) angular momenta, whose relaxation, in turn, is governed by operator (4). This assumption is consistent with classical molecular dynamics simulations, in which one integrates equations of motion of the kind

$$\partial_t D^j(\boldsymbol{\Omega}) = -i \hat{\Lambda}_{\boldsymbol{\Omega}} D^j(\boldsymbol{\Omega}), \quad \partial_t \mathbf{J} = -i \hat{\Lambda}_{\mathbf{J}} \mathbf{J} + \mathbf{N},$$

$D^j(\Omega)$ being the Wigner D-functions⁶³ and \mathbf{N} being the torque acting on a chosen molecule from its neighbours. As is demonstrated below, \mathbf{N} is essentially non-Gaussian and non-Markovian.

The operator \hat{C} can further be represented in the general form³³

$$\hat{C}(\mathbf{J})\rho(\mathbf{J}, \Omega, t) = -\nu\{\rho(\mathbf{J}, \Omega, t) - \int d\mathbf{J}' T(\mathbf{J}|\mathbf{J}')\rho(\mathbf{J}', \Omega, t)\}. \quad (7)$$

The rate ν determines the dissipation strength, and the relaxation kernel T obeys the normalization

$$\int d\mathbf{J} T(\mathbf{J}|\mathbf{J}') = 1 \quad (8)$$

and the detailed balance

$$T(\mathbf{J}|\mathbf{J}')\rho_B(\mathbf{J}') = T(\mathbf{J}'|\mathbf{J})\rho_B(\mathbf{J}), \quad (9)$$

$$\rho_B(\mathbf{J}) = (2\pi)^{-3/2} \exp\{-J_\alpha^2/(2I_\alpha)\} \quad (10)$$

being the equilibrium rotational Boltzmann distribution.

To proceed further, we adopt the KSM parametrization of the relaxation kernel^{33,64}:

$$T(\mathbf{J}|\mathbf{J}') = \prod_{a=x,y,z} T_a(J_a|J'_a), \quad (11)$$

$$T_a(J_a|J'_a) = [2\pi I_a(1 - \gamma_a^2)]^{-1/2} \exp\{-(J_a - \gamma_a J'_a)^2/[2I_a(1 - \gamma_a^2)]\}.$$

Here the parameters $-1 \leq \gamma_a \leq 1$ determine the relaxation mechanisms. When $\gamma_a = 1$, then $T_a(J_a|J'_a) = \delta(J_a - J'_a)$ and $\hat{C}(\mathbf{J}) = 0$. The Fokker-Planck relaxation operator is recovered in the limit $\gamma_a \rightarrow 1$, $\nu \rightarrow \infty$, $\nu(1 - \gamma_a) \rightarrow \nu_a = \text{const}$. If $\gamma_a = 0$, intermolecular interactions are so strong that they “immediately” restore an equilibrium Boltzmann distribution in the molecular ensemble ($T(\mathbf{J}|\mathbf{J}') \rightarrow \rho_B(\mathbf{J})$). Therefore, the KSM contains the J-diffusion model^{34,35,36,37,38,39,40,41,42} and the rotational Fokker-Planck equation^{24,35,36,43,44,45} as special cases.

By letting $\gamma_a = -1$, one gets $T_a(J_a|J'_a) = \delta(J_a + J'_a)$. Thus the magnitude of the angular momentum is preserved but its direction is reversed. This regime ($\gamma_a \simeq -1$, a molecule rotates back and forth within the cage formed by its nearest neighbors) is expected to be of particular relevance for hydrogen-bonding liquids. Such physical picture of molecular

reorientation in liquids is inherent in a number of theoretical approaches, in which the influence of the nearest neighbors on the selected molecule is modeled by external potentials with several minima^{26,27,47,65,66,67,68,69,70,71}, or by fluctuating torques and structures^{12,28,55}. Within the present approach, the fluctuating cage potential is not introduced explicitly, but its influence is taken into account dynamically via kernel (11).

Before embarking at particular calculations, it is useful to estimate values of the parameters ν , γ_a (Eq. (11)) and λ_i (Eq. (5) for hydrogen-bonding liquids. Since the molecules are assumed to undergo hindered librations, one expects $\nu \gg 1$ and $\gamma_a \sim -1$. The memory effects are supposed to be quite significant ($\lambda_i \sim 1$).

III. CORRELATION FUNCTIONS

After the explicit form of the relaxation operator (11) has been determined, the master equation (1) can be invoked to calculate any rotational and/or orientational CF of interest. To study the evolution of any quantity, which depends solely on the angular momentum, we integrate Eq. (1) over Ω and obtain the reduced master equation

$$\partial_t \rho(\mathbf{J}, t) = -i\hat{\Lambda}_{\mathbf{J}}\rho(\mathbf{J}, t) - \int_0^t dt' g(t-t')\hat{C}(\mathbf{J})\rho(\mathbf{J}, t'). \quad (12)$$

OCF of the rank j is defined through the Wigner D-functions as follows:

$$G^j(t) \equiv \langle D^j(\Omega(t))D^j(\Omega(0))^{-1} \rangle \equiv \int d\mathbf{J} G^j(\mathbf{J}, t). \quad (13)$$

After the insertion of the above definition into Eq. (1) one obtains the following equation:

$$\partial_t G^j(\mathbf{J}, t) = -i(\Lambda_{\Omega} + \hat{\Lambda}_{\mathbf{J}})G^j(\mathbf{J}, t) - \int_0^t dt' g(t-t')\hat{C}(\mathbf{J})G^j(\mathbf{J}, t'). \quad (14)$$

Here operator $\Lambda(\mathbf{J})$ is determined by Eqs. (2) and (3), in which the angular momentum operators \hat{L}_{α} are replaced by their matrix elements L_{α}^j over the D-functions:

$$(L_x^j)_{kl} \pm i(L_y^j)_{kl} = \delta_{k,l\mp 1} \{(j \pm l)(j \mp l + 1)\}^{1/2}, \quad (L_z^j)_{kl} = l\delta_{kl}; \quad -j \leq k, l \leq j. \quad (15)$$

Eqs. (12) and (14) can be solved numerically in case if a general asymmetric top molecule. To make the presentation simpler, we restrict ourselves to the consideration of spherically symmetric molecules. The corresponding formulas are much more elucidating and convenient

to analyse, since the relaxation operator $\hat{C}(\mathbf{J})$ is described by only two dynamic parameters (the intensity, ν , and the efficiency, γ , of dissipation) and a spherical molecule possesses a single moment of inertia, I . This theory can be applied to asymmetric tops as well. Indeed, in the hindered rotation limit ($\tau_J \ll 1$), a molecule librates back and forth in its cage, and every single libration reorients the molecule to a small angle. Using the explicit form of the operator $\hat{\Lambda}_{\Omega}$ (3), it is easy to demonstrate that the averaged inertial reorientation angle of an asymmetric top around its z -axis equals $(t/\tau_r)^2 \ll 1$, where

$$\tau_r = \sqrt{I/(k_B T)}, \quad I^{-1} = (I_x^{-1} + I_y^{-1})/2. \quad (16)$$

This corresponds to the rotation of the spherical molecule with the effective moment of inertia I . Thus, all the formulas obtained below can be used for asymmetric top molecules by making use of the substitution (16), provided one is interested in the orientational relaxation of the tensor with nonzero components along the molecular z -axis. If the quantity under study possesses nonzero components along several axes of the main moments of inertia (like OH stretch in HOD), the above analysis remains true if the effective moment of inertia I is modified accordingly. On the contrary, free inertial rotation of spherical, symmetric and asymmetric tops is very different^{72,73,74}.

Starting from Eq. (12), it is straightforward to derive the explicit formulas for the Laplace transformations of the angular momentum and rotational energy CFs:

$$C_J(t) = \frac{\langle \mathbf{J}\mathbf{J}(t) \rangle}{\langle \mathbf{J}^2 \rangle}, \quad \tilde{C}_J(s) = \frac{1}{s + \nu_J \tilde{g}(s)}, \quad (17)$$

$$C_E(t) = \frac{\langle \mathbf{J}^2 \mathbf{J}^2(t) \rangle - \langle \mathbf{J}^2 \rangle^2}{\langle \mathbf{J}^4 \rangle - \langle \mathbf{J}^2 \rangle^2}, \quad \tilde{C}_E(s) = \frac{1}{s + \nu_E \tilde{g}(s)}. \quad (18)$$

Here the rates

$$\nu_J = \nu(1 - \gamma), \quad \nu_E = \nu(1 - \gamma^2) \quad (19)$$

determine the angular momentum and rotational energy integral relaxation times:

$$\tau_J = \int_0^\infty dt C_J(t) = \tilde{C}_J(0) = \nu_J^{-1}, \quad (20)$$

$$\tau_E = \int_0^\infty dt C_E(t) = \tilde{C}_E(0) = \nu_E^{-1}. \quad (21)$$

As to the OCFs, the solution of Eq. (14) can be given in terms of recursive relationships (or, equivalently, in terms of continued fractions) for any value of the relaxation parameters ν and γ , as well as for any memory function $g(t)$, see Appendix A.

IV. ILLUSTRATIVE CALCULATIONS

In this Section, we present and discuss the results of representative calculations of the angular momentum CFs (17), energy CFs (18), and OCFs (29) - (33) within the NKSM. The free rotation period (16) has been taken as $\tau_r = \sqrt{I/(k_B T)} = 93$ fs. This corresponds to *HOD* at $T = 300$ K ($I_x = 2.63$, $I_y = 1.85$, $I_z = 0.72$ a.m.u. $\times \text{\AA}^2$).

We start from the angular momentum (17) and energy (18) CFs. If the two-exponential memory function (5) is used, the Laplace images $\tilde{C}_J(s)$ and $\tilde{C}_E(s)$ can be inverted into the time domain by solving the pertinent cubic equation. The CFs in the time domain are thus determined by linear combinations of one real and two complex conjugated exponentials. The results of representative calculations are depicted in Fig. 1. A decrease of the second memory parameter, λ_2 , causes a typical transformation of the angular momentum CF, which reflects a passage from simple to hydrogen-bonding liquids²⁵. Since CFs $C_J(t)$ attain negative values, their actual decay occur at a timescale of several hundreds of femtosecond, which is much longer than the integral relaxation time $\tau_J = \nu_J^{-1} = 4.65$ fs. The rotational energy CFs are monotonous and decay at a much longer time scale of $10 \div 15$ ps, which is a direct manifestation of the librational motion ($\gamma \sim -1$, $\tau_J \ll \tau_E$).

Let us turn to the study of orientational relaxation. To get a qualitative feeling of the influence of the relaxation efficiency γ on molecular reorientation, let us concentrate on the long-time behavior of OCFs and consider the Markovian limit, $g(t) \rightarrow \delta(t)$. As has been established in^{52,53}, the KSM predicts that the smaller is γ , the slower is the OCF decay. Thus, for a fixed angular momentum relaxation rate ν_J , the rotational Fokker-Planck equation ($\gamma = 1$) predicts the most rapid orientational relaxation, while the limit of perfect librations ($\gamma = -1$) corresponds to the slowest orientational relaxation. This is clearly seen in Fig. 2.

As is demonstrated in Appendix B, Eq. (14) can be solved analytically for OCFs in case

of perfect forward-backward librations ($\gamma = -1$) in the hindered rotation limit ($\nu \gg 1$):

$$G^j(t) = \frac{1}{2j+1} \left(1 + 2 \sum_{k=1}^j \left[1 + \frac{k^2}{\nu} t \right]^{-3/2} \right). \quad (22)$$

On the scale of Fig. 2, the exact solution of Eq. (14) in the limit of $\gamma = -1$ and the approximate one, which is delivered by Eq. (22), are indistinguishable. Thus the in-cage librations manifest themselves through a slow algebraic $t^{-3/2}$ decay of the OCF. This behavior is caused by the angular momentum reversion ($\gamma = -1$) and has nothing in common with long-time hydrodynamic tails of the angular velocity CFs of Brownian particles (see^{12,75,76} and references therein)⁷⁷. It is interesting to point out that the OCFs calculated within the M-^{39,78} and E-⁴¹ diffusion models exhibit similar ($\sim t^{-3/2}$) long time tails, which are commonly regarded as unphysical. Nonetheless, these models were successfully invoked to reproduce “experimental” OCFs, which were obtained through the inversion of IR and Raman spectra into the time domain^{41,78,79,80,81}. The present consideration reveals that this success is not accidental, since the conservation of the magnitude of the angular momentum (M- diffusion) or rotational energy (E- diffusion) mimics the description of in-cage librations via the KSM kernel (11), which in the limit $\gamma \sim -1$ conserves both of these quantities.

Fig. 3 illustrates the influence of the memory effects, which modify the short-time behavior of the OCFs. The mechanism of this influence is uncovered by the general expression²⁴

$$G^j(t) \approx 1 - j(j+1) \int_0^t dt' (t-t') C_J(t'), \quad (23)$$

which relates the short-time OCF behavior with the time evolution of the angular momentum CF. That is why the parameters which have been used for the calculation of the OCFs in Fig. 3 and the angular momentum CFs in Fig. 1a are the same. Generally, the memory effects speed up the short-time OCF decay. If the angular momentum CF is highly oscillatory, these oscillations show up in OCFs also (compare dotted lines in Figs. 1a and 3).

OCFs depicted in Fig. 3 look qualitatively similar to those obtained via computer simulations^{4,5,12,15,82,83}. A more quantitative comparison of the simulated and NKSM OCFs is presented in Fig. 4. It depicts the results of molecular dynamic simulations of the first (upper dotted line) and second (lower dotted line) rank OCFs for *HOD* in D_2O at a room temperature using the SPC/E model for water⁵ along with the fits obtained within the NKSM (full lines). Detail of the molecular dynamics simulation protocol can be found in ref.^{4,84}

The present theory is seen to reproduce the simulated OCFs quite well. We were unable, however, to fit the first and second rank OCFs by the same set of the NKSM parameters. This is not unexpected: OCFs of different ranks are affected by the cage potentials in a different way, which is determined by the potential symmetry⁵⁵. The dielectric friction, which governs orientational relaxation in polar systems is also known to be rank-dependent⁸⁵. The values of ν , γ , λ_i and σ which are extracted from the angular momentum CF deliver, in fact, certain averaged values. It is nonetheless quite remarkable that the parameters which have been used for the calculation of the second rank OCF are identical to those which have been used for the computation of the angular momentum CF (Fig. 1a, full line). This latter CF looks very similar to the simulated one¹⁵.

Fig. 5 shows the normalized anisotropy extracted from the pump-probe signal⁵ (dotted line). It deviates quite significantly from the simulated second-rank OCF (our best fit to this OCF is plotted here for the sake of comparison). As has been pointed out in^{4,5,83}, simulations normally predict faster, in comparison with experiment, anisotropy decays. This is caused, perhaps, by ignoring either the water polarizability^{86,87} or quantum effects¹⁵. We are not attempting to resolve this controversy here. Note merely that the experimental anisotropy can be fitted quite well within the NKSM (full line), with the set of parameters which predict more “librational” reorientation (γ is closer to -1) and more pronounced memory effects (λ_i is smaller).

Let us return back to Fig. 4. The OCFs calculated within the standard diffusion equation,

$$G^j(t) = \exp\{-j(j+1)\tau_J t\}, \quad (24)$$

which reproduces the long-time limit of the first cumulant formula,

$$G^j(t) = \exp\{-j(j+1) \int_0^t dt' (t-t') C_J(t')\}, \quad (25)$$

are seen to deviate significantly from the simulated/NKSM OCFs. Despite the simulated/NKSM OCFs do exhibit the long-time exponential behavior, and despite the rotational motion is definitely hindered ($\tau_J \ll 1$), the diffusion equation cannot reproduce these OCFs. The failure of the diffusion equation has quite an evident explanation. If we assume that the molecules undergo “perfect” librations ($\gamma = -1$ within the present theory), then the long-time behavior of the OCF in the hindered rotation limit is described by Eq. (22) rather than by the small-angle diffusion equation (24). Since the actual librations are not

“perfect” (γ is close to but less than -1) one expects deviations from Eq. (22). As is seen from Fig. 6, this is indeed the case. This Figure reproduces the Markovian limits of the KSM OCFs from Figs. 4 and 5, along with their counterparts calculated via Eq. (22). The short-to-intermediate-time resemblance of the OCFs is quite remarkable.

On the other hand, the long-time behavior of the simulated/KSM OCFs is seen to be exponential and is not reproduced by Eq. (22). This hints at a possibility that rotational energy relaxation might be responsible for the long time exponential decay of the simulated/NKSM OCFs. This hypothesis is corroborated by the observation that the fit of the simulated and NKSM OCFs of the first and second rank (Fig. 4) delivers different values of the relaxation parameters ν and γ . However, the quantity $\nu_E = \nu(1 - \gamma^2) = 0.027$ turns out to be the same for both $j = 1$ and 2. This gives the estimated value of 3.4 ps for the rotational energy relaxation time τ_E . This value correlates with the experimentally measured long time anisotropy decay times of $2 \div 3$ ps^{4,5,6,7,9,10}.

Note, finally, that a close interrelation between the hydrogen bond dynamics and rotation dynamics has repeatedly been emphasized in the literature. The NKSM values of the “persistence time” of the oscillatory angular momentum CF (Fig. 1a) and the rotational energy relaxation time, ~ 150 fs and 3.4 ps, correlate quite well with the estimations for the continuous and intermittent hydrogen bond lifetimes^{83,88}. This observation is consistent with the physical picture of molecular rotation underlying the NKSM approach. The in-cage librations, which can cause bond breakings, manifest themselves on the time scale of the “persistence time” of the angular momentum CF. On the other hand, the bond rupturings are accompanied by subsequent bond reformings, since the molecule does not leave its local cage. A “true” cleavage of the bond can occur on the τ_E timescale since, within the NKSM description, the rotational energy relaxation occurs due to a hopping to a new position of the local equilibrium or restructuring the local potential well.

V. CONCLUSION

We have developed a NKSM description of the orientational relaxation in hydrogen-bonding liquids. Within the NKSM, molecular rotation is governed by two relaxation parameters ν and γ (which describe the intensity and mechanism of dissipation), as well as by the memory function $g(t)$ (5), which is responsible for the short-time dynamics. Alter-

natively, the relaxation parameters ν and γ are uniquely determined through the angular momentum and energy relaxation times τ_J (20) and τ_E (21). Once a set of the parameters is selected, the NKSM allows to calculate any rotational CF or OCF of interest. Keeping in mind a considerable success of the KSM in reproducing molecular reorientation in gases^{33,51}, the results of the present work demonstrate that the NKSM can be used for the description and interpretation of the orientational relaxation in a condensed phase, from rarefied gases with binary collisions, through dense fluids to hydrogen-bonding liquids.

The NKSM suggests the short-time relaxation of the OCFs in the hydrogen-bonding liquids is described by an algebraic $\sim t^{-3/2}$ contribution. This algebraic behavior is modified by more rapid and non-monotonous dynamics, which is induced by the memory effects. The long-time decay of the OCFs is exponential, although non-diffusional. It is governed by the rotational energy relaxation time, τ_E . Our results are contrary to standard belief that the angular momentum CF determines molecular reorientation in the hindered rotation limit, and the first cumulant expression, Eq. (25), delivers the leading contribution into the OCF. Our results indicate, that knowing $C_J(t)$ is not enough to predict OCFs for hydrogen-bonding liquids, since the long-time behavior of OCFs is governed by the rotational energy CF, $C_E(t)$.

It is a conventional practice to fit various experimental or simulated CFs via a linear combination of several real (if the CF decays monotonously) or complex (if the CF exhibits oscillatory behavior) exponents. According to the present analyses, the OCF in hydrogen-bonding liquids contains an algebraic $\sim t^{-3/2}$ contribution. This finding suggests that the following fitting formulas for the angular momentum CF,

$$C_J(t) = a_1 \exp\{-\nu_1 t\} + \exp\{-\nu_2 t\} (a_2 \cos(\Omega t) + a_3 \sin(\Omega t)), \quad (26)$$

and for the OCF,

$$G^j(t) = b_1 \exp\{-\nu_1 t\} + \exp\{-\nu_2 t\} (b_2 \cos(\Omega t) + b_3 \sin(\Omega t)) + b_4 \exp\{-\nu_3 t\} [1 + b_5 t]^{-3/2} + b_6 \exp\{-\nu_4 t\}, \quad (27)$$

can be more physically motivated (a_i , b_i , ν_i and Ω being certain real-valued parameters). Indeed, Eq. (26) is nothing else than a formal solution of Eq. (17) in the case of two-exponential memory function (5). As to the OCF (27), the first three terms with coefficients

b_1, b_2, b_3 describe the angular momentum induced short-time rapid decay and oscillations. The term which is proportional to b_4 is responsible for the algebraic contribution, and the last term governs the long-time exponential decay.

Acknowledgments

The authors are grateful to Joseph Loparo for sending them the numerical data on the simulated OCFs and measured anisotropies, which have been published in⁵. M. F. G. thanks Alexander Blokhin for numerous stimulating and useful discussions.

VI. APPENDIX A. RECURSIVE RELATIONS FOR LINEAR AND SPHERICAL TOP OCFs

After being Laplace transformed, Eq. (14) reads:

$$-\rho_B(\mathbf{J}) + s\tilde{G}^j(\mathbf{J}, s) = -i(\Lambda_\Omega + \hat{\Lambda}_\mathbf{J})\tilde{G}^j(\mathbf{J}, t) - \nu\tilde{g}(s)\{\tilde{G}^j(\mathbf{J}, s) - \int d\mathbf{J}' T(\mathbf{J}|\mathbf{J}')\tilde{G}^j(\mathbf{J}', s)\}. \quad (28)$$

Since Eq. (28) depends on s parametrically, the method of its solution in the Markovian limit ($\tilde{g}(s) = 1$), which has been developed in^{35,46,51,52}, is directly applicable to the present case also. One has merely consider the complex quantity $\nu g(s)$ as the generalized relaxation rate. We therefore present the final expressions for the calculation of the first and second rank OCFs.

Their Laplace images of the spherical top OCFs can be calculated via the formula

$$\tilde{G}^j(s) = (1 + 2b_0)/s. \quad (29)$$

For $j = 1$, the coefficient b_0 can be retrieved from the simple three-term recursive formula^{35,52}

$$\frac{1}{s}\delta_{m0} = \frac{4m + 10}{\sigma_{m+1}}b_{m+1} - \left\{ \frac{2m + 3}{\sigma_{m+1}} + \frac{2m + 2}{\sigma_m} + \zeta_m \right\} b_m + \frac{m}{\sigma_m}b_{m-1}, \quad (30)$$

δ_{m0} being the Kronecker delta. The value of b_0 for the second rank OCF can be extracted from the system of coupled recursive relations for the coefficients b_m and d_m ⁵²:

$$\begin{aligned} \frac{1}{s}\delta_{m0} = & - \left\{ \frac{6}{\sigma_m} + \zeta_m \right\} b_m + \frac{12}{\sigma_{m+1}}b_{m+1} \\ & - \frac{4m}{\sigma_m}d_{m-1} + \left\{ \frac{8m - 14}{\sigma_m} + \frac{8m - 31}{\sigma_{m+1}} \right\} d_m + \frac{-16m^2 + 74m + 12}{(m + 1)\sigma_{m+1}}d_{m+1}; \end{aligned} \quad (31)$$

$$0 = \frac{m}{\sigma_m} b_{m-1} - \left\{ \frac{2m-1}{\sigma_m} + \frac{2m-1}{\sigma_{m+1}} \right\} b_m + \frac{4m}{\sigma_{m+1}} b_{m+1} \\ + \frac{5m}{\sigma_m} d_{m-1} - \left\{ \frac{14}{\sigma_m} + \frac{4+10m}{\sigma_{m+1}} + \zeta_m \right\} d_m + \frac{4m(9+5m)}{(m+1)\sigma_{m+1}} d_{m+1}. \quad (32)$$

Here

$$\sigma_m \equiv s + \nu \tilde{g}(s)(1 - \gamma^{2m}), \quad \zeta_m \equiv s + \nu \tilde{g}(s)(1 - \gamma^{2m+1}). \quad (33)$$

The solution of the recursive relations for the first rank OCF (30) can be expressed in the continued fraction form³⁵, while the solution of Eqs. (31) and (32) for the second-rank OCF can be given in terms of the matrix 2×2 continued fractions⁸⁹.

The first and second rank OCFs for linear rotors can be evaluated very similarly, through the simple three-term recursive formulas. Namely, the Laplace images of the OCFs can also be computed via Eq. (29). For $j = 1$, the coefficient b_0 must be determined by the formula^{35,51}

$$\frac{1}{s} \delta_{m0} = \frac{4m+8}{\sigma_{m+1}} b_{m+1} - \left\{ \frac{2m+2}{\sigma_{m+1}} + \frac{2m+2}{\sigma_m} + \zeta_m \right\} b_m + \frac{m}{\sigma_m} b_{m-1},$$

while the second-rank OCF ($j = 2$) can be computed through⁵¹

$$\frac{3}{s} \delta_{m0} = \frac{16m+32}{\sigma_{m+1}} b_{m+1} - \left\{ \frac{8m+10}{\sigma_{m+1}} + \frac{8m+6}{\sigma_m} + \zeta_m \right\} b_m + \frac{4m}{\sigma_m} b_{m-1}.$$

VII. APPENDIX B. ORIENTATIONAL RELAXATION IN CASE OF PERFECT ANGULAR MOMENTUM REORIENTATION

If we neglect the memory effects ($g(t) \rightarrow \delta(t)$) and put $\gamma = -1$, then Eq. (14) can be solved analytically:

$$G^j(t) = \frac{1}{2j+1} \int_0^\infty dJ \rho_B(J) \\ \times \left(1 + \exp\{-\nu t\} \sum_{k=1}^j [(1 + \nu/\omega_k) \exp\{\omega_k t\} + (1 - \nu/\omega_k) \exp\{-\omega_k t\}] \right). \quad (34)$$

The frequencies are explicitly defined as follows

$$\omega_k = \sqrt{\nu^2 - k^2 J^2}. \quad (35)$$

Several important properties of Eq. (34) are to be discussed. OCF (34) possesses a stationary asymptote: $G^j(t \rightarrow \infty) = (2j + 1)^{-1}$, which is identical to the free OCF asymptote. This can be easily understood: reversion of the angular momentum is equivalent to the reversion of the sense of molecular rotation. Therefore a sequence of forward-backward rotations is equivalent to a single free rotation. This asymptote is solely caused by dynamic effects (in-cage librations, compare with⁶⁵) rather than by external potentials (see, e.g.,^{9,90,91}). The librational motion itself is caused, of course, by in-cage potentials but they do not enter explicitly into our analysis. If $\nu \rightarrow 0$, Eq. (34) reproduces the free spherical top OCF. If we take the opposite limit $\nu \rightarrow \infty$, then $G^j(t) \rightarrow 1$ since a large number of small-angle forward-backward rotations causes no net reorientation. In the hindered rotation limit ($\tau_J \ll 1$) Eq. (34) reduces to (22).

Using the explicit form of the free linear rotor OCF⁷² one can easily derive the linear rotor counterpart of Eq. (22):

$$G^j(t) = \left(d_{00}^j\left(\frac{\pi}{2}\right)\right)^2 + 2 \sum_{k=1}^j \left(d_{0k}^j\left(\frac{\pi}{2}\right)\right)^2 \left[1 + \frac{k^2}{\nu_l} t\right]^{-1}, \quad (36)$$

$d_{km}^j(\beta)$ being the reduced Wigner function⁶³. It is well known that the exponent d of the long-time hydrodynamic tails $t^{-d/2}$ of the angular velocity CFs of Brownian particles is determined by the dimensionality of the rotation space: $d = 3$ for any spherical, symmetric or asymmetric top while $d = 2$ for a linear rotor (75,76 and references therein). This general statement holds true in the present case also, and OCF (36) possesses a $\sim t^{-1}$ tail. This means that the algebraic contribution to OCF (36) decays slower than its $t^{-3/2}$ counterpart in the spherical top OCF (22). Furthermore, $d_{00}^j(\pi/2) = 0$ for odd j . Thus, the odd-ranked OCFs do not possess the stationary contribution and decay faster than the even-ranked OCFs.

¹ J. S. Baskin and A. H. Zewail, *J. Phys. Chem. A* 105, 3680 (2001).

² R. Laenen, C. Rauscher and A. Laubereau, *Phys. Rev. Lett.* 80, 2622 (1998).

³ C. Ronne, P.-O. Astrand and S. O. Keiding, *Phys. Rev. Lett.* 82, 2888 (1999).

⁴ J. J. Loparo, C. J. Fecko, J. D. Eaves, S. T. Roberts, and A. Tokmakoff, *Phys. Rev. B* 70, 180201(R) (2004).

⁵ C. J. Fecko, J. J. Loparo, S. T. Roberts, and A. Tokmakoff, *J. Chem. Phys.* 122, 054506 (2005).

⁶ H.-K. Neinhuys, R. A. van Santen and H. J. Bakker, *J. Chem. Phys.* 112, 8487 (2000).

⁷ Y. L. A. Rezus and H. J. Bakker, *J. Chem. Phys.* 123, 114502 (2005).

⁸ T. Steinel, J. B. Asbury, J. Zheng and M. D. Fayer, *J. Phys. Chem. A* 108, 10957 (2004).

⁹ H.-S. Tan, I. R. Piletic, and M. D. Fayer, *J. Chem. Phys.* 122, 174501 (2005).

¹⁰ D. Cringus, S. Yeremenko, M. S. Pshenichnikov and D. A. Wiersma, *J. Phys. Chem. B* 108, 10387 (2004).

¹¹ G. Gallot, S. Bratos, S. Pommeret, N. Lascoux, J.-Cl. Leicknam, M. Kozinski, W. Amir and G. M. Gale, *J. Chem. Phys.* 117, 11301 (2002).

¹² M. P. Allen and D. J. Tildesley, *Computer Simulation of Liquids* (Clarendon Press, Oxford, 1991).

¹³ M. Sprik, J. Hutter and M. Parrinello, *J. Chem. Phys.* 105, 1142 (1996).

¹⁴ A. D. Boese, A. Chandra, J. M. L. Martin, and D. Marx, *J. Chem. Phys.* 119, 5965 (2003).

¹⁵ L. Hernndez de la Pea and P. G. Kusalik, *J. Chem. Phys.* 121, 5992 (2004).

¹⁶ L. D. Favro, *Phys. Rev.* 119, 53 (1960).

¹⁷ P. S. Hubbard, *J. Chem. Phys.* 52, 563 (1970).

¹⁸ W. T. Huntres, *Adv. Magn. Res.* 40, 1 (1970).

¹⁹ K. A. Valijev and E. N. Ivanov, *Uspekhi Fiz. Nauk* 109, 31 (1973).

²⁰ R. I. Cukier and K. Lakatos-Lindenberg, *J. Chem. Phys.* 57, 3427 (1972).

²¹ R. I. Cukier, *J. Chem. Phys.* 60, 734 (1974).

²² A. P. Blokhin and M. F. Gelin, *Physica A* 251, 469 (1998).

²³ W. A. Steele, *J. Chem. Phys.* 38, 2404 (1963); *ibid* 38, 2411 (1963).

²⁴ G. W. Ford, J. T. Lewis and J. McConnell, *Phys. Rev. A* 19, 907 (1979).

²⁵ R. M. Lynden-Bell, in *Molecular liquids*, edited by A. J. Barnes, W. J. Orville-Thomas and J.

Yarwood (NATO ASI Series C, V. 135, 1984), P. 501.

²⁶ R. M. Lynden-Bell and W. A. Steele, *J. Phys. Chem.* 88, 6514 (1984).

²⁷ V. N. Kabadi and W. A. Steele, *J. Phys. Chem.* 89, 1467 (1985).

²⁸ W. Coffey, M. Evans and P. Grigolini. *Molecular diffusion and spectra* (John Wiley & Sons, 1984).

²⁹ W. A. Steele, in *Molecular liquids*, edited by A. J. Barnes, W. J. Orville-Thomas and J. Yarwood (NATO ASI Series C, V. 135, 1984), P. 111.

³⁰ D. Kivelson and T. Keyes, *J. Chem. Phys.* 57, 4599 (1972).

³¹ D. Kivelson and R. Miles, *J. Chem. Phys.* 88, 1925 (1988).

³² E. Detyna, K. Singer, J. V. L. Singer and A. J. Taylor, *Mol. Phys.* 41, 31 (1980).

³³ A. I. Burshtein and S. I. Temkin. *Spectroscopy of Molecular Rotations in Gases and Liquids* (Cambridge University Press, Cambridge, 1994).

³⁴ R. G. Gordon, *J. Chem. Phys.* 44, 1830 (1966).

³⁵ R. A. Sack, *Proc. Phys. Soc. B.* 70, 402 (1957); *ibid* 70, 414 (1957).

³⁶ M. Fixman and K. Rider, *J. Chem. Phys.* 51, 2425 (1969).

³⁷ A. G. St. Pierre and W. A. Steele, *J. Chem. Phys.* 57, 4638 (1972).

³⁸ J.-Cl. Leicknam, Y. Guissani and S. Bratos, *J. Chem. Phys.* 68, 3380 (1978).

³⁹ R. E. D. McClung, *Adv. Mol. Rel. Int. Proc.* 10, 83 (1977).

⁴⁰ T. E. Bull and W. Egan, *J. Chem. Phys.* 81, 3181 (1984).

⁴¹ A. P. Blokhin and M. F. Gelin, *Khim. Fiz.* 17, No 12, 108 (1998).

⁴² M. Constan, R. Fauquembergue and P. Descheerde, *J. Chem. Phys.* 64, 667 (1976).

⁴³ P. S. Hubbard, *Phys. Rev. A.* 6, 2421 (1972).

⁴⁴ A. Morita, *J. Chem. Phys.* 76, 3198 (1982).

⁴⁵ D. H. Lee and R. E. D. McClung, *Chem. Phys.* 112, 23 (1987).

⁴⁶ A. P. Blokhin and M. F. Gelin, *Physica A* 229, 501 (1996).

⁴⁷ V. I. Gaiduk and Y. P. Kalmykov, *J. Chem. Soc., Faraday Trans. 2* 77, 929 (1981).

⁴⁸ W. A. Steele, *Mol. Phys.* 43, 141 (1981).

⁴⁹ A. P. Blokhin and M. F. Gelin, *Khim. Fiz.* 16, No 1, 39 (1997); *ibid* 16, No 1, 50 (1997).

⁵⁰ A. P. Blokhin and M. F. Gelin, *J. Phys. Chem. B* 101, 236 (1997).

⁵¹ M. F. Gelin, *J. Phys. Chem. A* 104, 6150 (2000).

⁵² A. P. Blokhin and M. F. Gelin, *Molec. Phys.* 87, 455 (1996).

⁵³ A. P. Blokhin and M. F. Gelin, *J. Molec. Liq.* 93, 47 (2001).

⁵⁴ Y. A. Serebrennikov, S. I. Temkin, A. I. Burshtein, *Chem. Phys.* 81, 31 (1983).

⁵⁵ A. Polimeno, G. J. Moro and J. H. Freed, *J. Chem. Phys.* 102, 8094 (1995); *ibid* 104, 1090 (1996).

⁵⁶ G. J. Moro and A. Polimeno, *J. Phys. Chem. B* 108, 9359 (2004).

⁵⁷ A. Magro, D. Frezzato, A. Polimeno, G. J. Moro, R. Chelli and R. Righini, *J. Chem. Phys.* 123, 124511 (2005).

⁵⁸ J. Jang and R. M. Stratt, *J. Chem. Phys.* 112, 7524 (2000); *ibid* 112, 7538 (2000).

⁵⁹ D. Laage and J. T. Hynes, *Science* 311, 832 (2006).

⁶⁰ G. T. Evans, *Mol. Phys.* 36, 65 (1978).

⁶¹ L.-P. Hwang and J. H. Freed, *J. Chem. Phys.* 63, 118 (1975).

⁶² For a more general (but complicated) description see^{22,33,60}.

⁶³ D. A. Varshalovich, A. N. Moskalev and V. K. Hersonski. *Quantum Theory of Angular Momentum* (World Scientific, Singapore, 1989).

⁶⁴ J. Keilson and J. E. Storer, *Quart. Appl. Math.*, 10, 243 (1952).

⁶⁵ S. Tang and G. T. Evans, *J. Chem. Phys.* 103, 1553 (1995).

⁶⁶ J. Frenkel, *Kinetic theory of fluids* (Dover, New York, 1955).

⁶⁷ F. J. Bartoli and T. A. Litovitz, *J. Chem. Phys.* 56, 413 (1972).

⁶⁸ J. N. Kushick, *J. Chem. Phys.* 67, 2068 (1977).

⁶⁹ E. Praestgaard and N.G. van Kampen, *Mol. Phys.* 43, 33 (1981).

⁷⁰ S. K. Deb, *Chem. Phys.* 120, 225 (1988).

⁷¹ Yu. Georgievskii and A. I. Burshtein, *J. Chem. Phys.* 101, 10858 (1994).

⁷² A. G. St. Pierre and W. A. Steele, *Phys. Rev.* 184, 172 (1969).

⁷³ A. P. Blokhin, *Vesti AN BSSR, Ser. fiz.-mat.* 2, 70 (1986); *ibid* 4, 77 (1986).

⁷⁴ M. Aguado-Gomez and J.-Cl. Leicknam, *Phys. Rev. A* 34, 4195 (1986); *ibid* A 35, 286 (1987).

⁷⁵ B. Cichocki and B. U. Felderhof, *J. Chem. Phys.* 107, 291 (1997).

⁷⁶ A. J. Masters, *J. Chem. Phys.* 107, 292 (1997).

⁷⁷ Strictly speaking, these hydrodynamic long-time tails are associated with local structures and confining potentials in liquids, but these effects are evidently not taken into account within the NKSM description.

⁷⁸ S. K. Deb and K. V. Bhagwat, *Chem. Phys.* 98, 251 (1985).

⁷⁹ W. G. Rothschild, G. J. Rosasco, R. C. Livingston, *J. Chem. Phys.* 62, 1253 (1975).

⁸⁰ S. Perry, T. W. Zerda, J. Jonas, *J. Chem. Phys.* 75, 4214 (1981).

⁸¹ C. Dreyfus, C. Breuillard, T. Nguyen-Tan, R. Ouillon, *Chem. Phys. Lett.* 62, 246 (1979).

⁸² I. M. Svischev and P. G. Kusalik, *J. Phys. Chem.* 98, 728 (1994).

⁸³ C. P. Lawrence and J. L. Skinner, *J. Chem. Phys.* 118, 264 (2003).

⁸⁴ J. D. Eaves, PhD thesis, Massachusetts Institute of Technology, 2004.

⁸⁵ S. Ravichandran and B. Bagchi, *J. Phys. Chem.* 98, 2729 (1994).

⁸⁶ H. Hu, H. A. Stern and B. J Berne, *J. Phys. Chem. B* 106, 2054 (2002).

⁸⁷ A. Chandra and T. Ichiye, *J. Chem. Phys.* 111, 2701 (1999).

⁸⁸ A. Luzar, *J. Chem. Phys.* 113, 10633 (2000).

⁸⁹ H. Risken. *The Fokker-Planck Equation* (Springer, Berlin, 1984).

⁹⁰ J. Helbing, K. Nienhaus, G. U. Nienhaus, P. Hamm, *J. Chem. Phys.* 122, 124505 (2005).

⁹¹ A. Szabo, *J. Chem. Phys.* 81, 150 (1984).

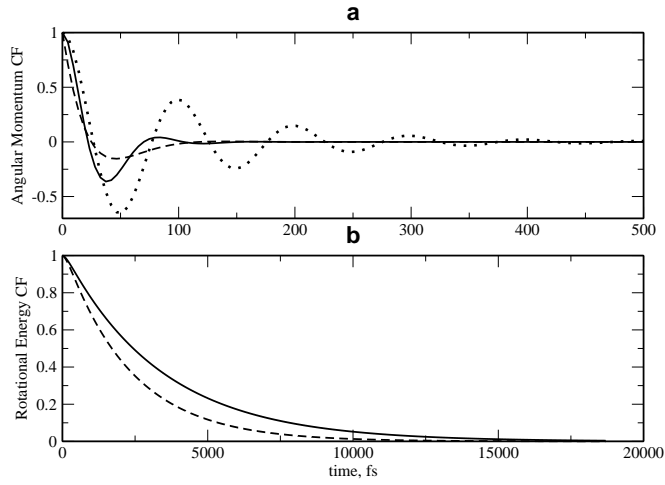


FIG. 1: Angular momentum (a) and energy (b) CFs for $\nu = 16$, $\gamma = -0.99915$ (that is $\nu_J = 32$ and $\nu_E = 0.027$), $\sigma = 0.2$ and $\lambda_1 = 0.7$. The dashed, full and dotted lines correspond to $\lambda_2 = 1000$, 10 and 3, respectively. On the scale of the figure, the rotational energy CFs for $\lambda_2 = 10$ and 3 are indistinguishable.

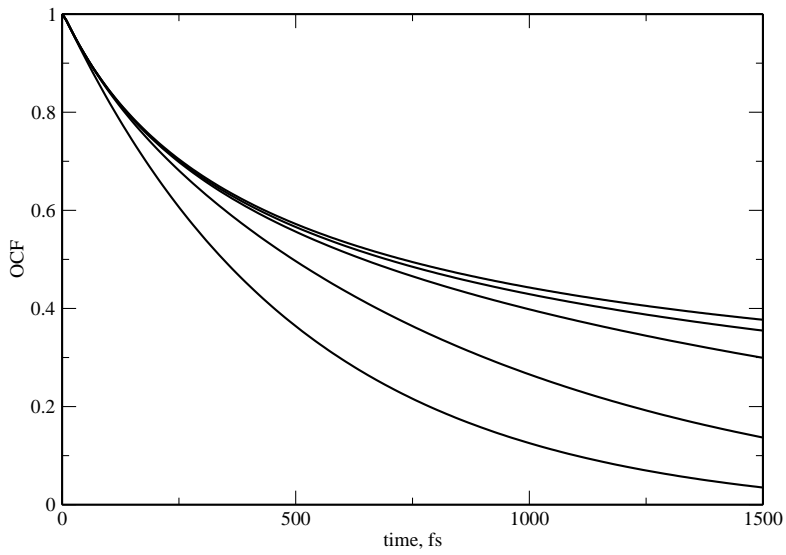


FIG. 2: The second rank OCFs in the Markovian limit for the relaxation rate rate $\nu_J = 32$. From bottom to top, the curves correspond to $\gamma = 1, -0.99, -0.999, -0.9999$ and 1 .

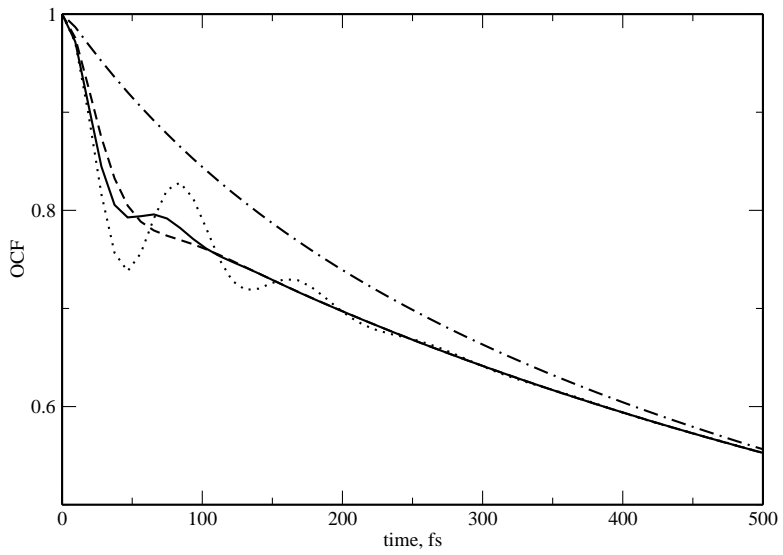


FIG. 3: The influence of the memory effects on the second rank OCFs. $\nu_J = 32$, $\gamma = -0.999$, $\sigma = 0.2$ and $\lambda_1 = 0.7$; $\lambda_2 = 1000$ (dashed lines), 10 (full lines) 3 (dotted lines). The dash-dotted curve depicts the OCF in the Markovian limit.

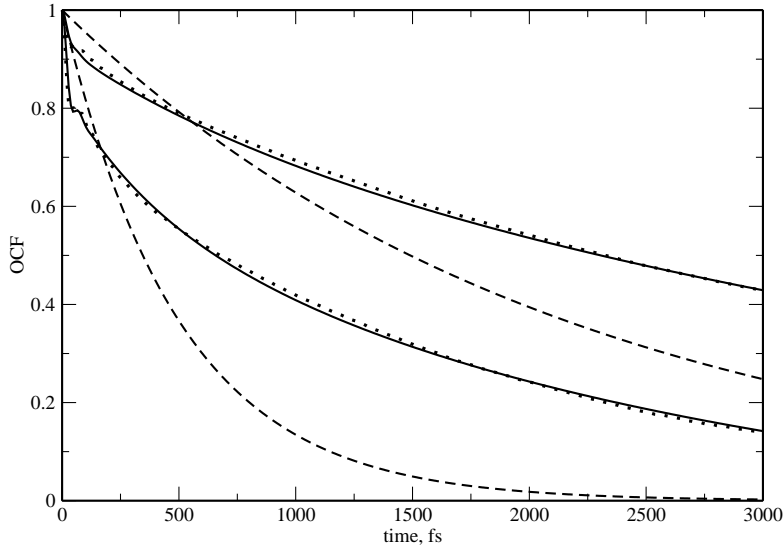


FIG. 4: Comparison of the simulated OCFs with those calculated within the NKSM. The dotted lines correspond to the first (upper curve) and second (lower curve) rank OCFs which were simulated for *HOD* in liquid D_2O at a room temperature⁵. The black curves are computed for $\nu_J = 46$, $\gamma = -0.999415$, $\sigma = 0.2$, $\lambda_1 = 0.4$, $\lambda_2 = 10$ ($j = 1$); $\nu_J = 32$, $\gamma = -0.99915$, $\sigma = 0.2$, $\lambda_1 = 0.7$, $\lambda_2 = 10$ ($j = 2$). The OCFs calculated via the diffusion equation (24) are depicted by dashed lines.

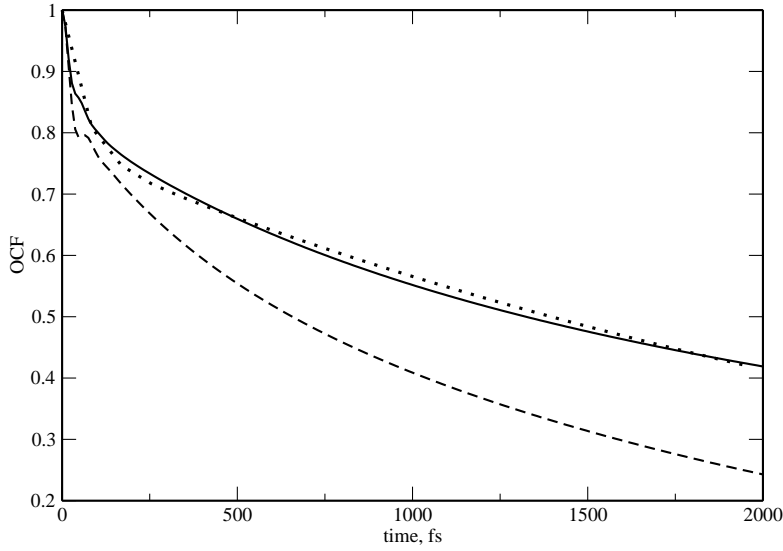


FIG. 5: Comparison of the experimental OCFs with those calculated within the NKSM. The dotted line reproduces the best fit to the experimental anisotropy decay⁵. The solid black curve shows the second-rank OCF computed within the NKSM for $\nu_J = 63$, $\gamma = -0.99995$, $\sigma = 0.2$, $\lambda_1 = 0.3$, $\lambda_2 = 10$. The dashed line reproduces the second rank NKSM OCFs from Fig. 4.

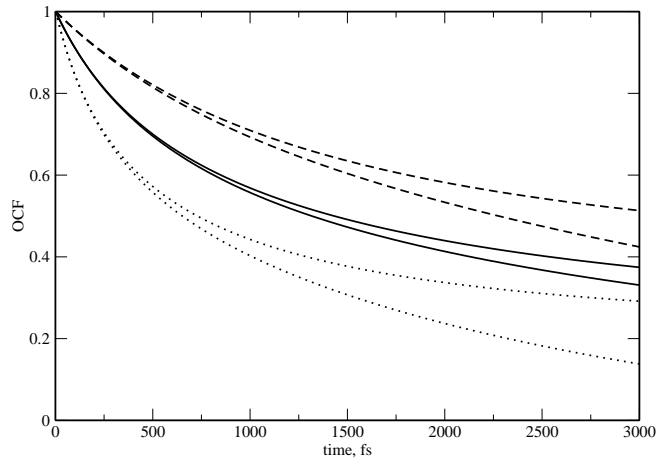


FIG. 6: Elucidation of the algebraic contributions into OCFs. For each couple of the curves, the upper one is calculated via Eq. (22) and the lower one is computed within the Markovian limit of the NKSM. The dotted ($j = 2, \nu_J = 32, \gamma = -0.99915$) and dashed ($j = 1, \nu_J = 46, \gamma = -0.999415$) curves correspond to the best-fit NKSM OCFs from Fig. 4, and the solid curves ($j = 2, \nu_J = 63, \gamma = -0.99995$) correspond to the best-fit NKSM OCFs from Fig. 5.